Materials Science-Poland, 41(3), 2023, pp. 111-125
http://www.materialsscience.pwr.wroc.pl/
DOI: 10.2478/msp-2023-0036

Effect of saccharin addition on formation, wear and corrosion resistance of electrodeposited Ni-Cr coatings

Mehmet Demir[1,*], Erdoğan Kanca[1], İsmail Hakki Karahan[2]

[1]Department of Mechanical Engineering, Faculty of Engineering and Natural Sciences, Iskenderun Technical University, 31200 Hatay, Turkey

[2]Department of Physics, Faculty of Arts and Sciences, Mustafa Kemal University, 31040, Hatay, Turkey

Numerous factors play a pivotal role in shaping the mechanical and corrosion resistance properties of electrodeposited Ni-Cr alloy coatings. This study delves into the deposition of Ni-Cr alloy coatings on AISI 1040 steel, examining the influence of saccharin additives within the electrodeposition bath. Specifically, the concentration of saccharin within the solution was varied over a range of 0 to 2 g/l. Following the electrodeposition process, a comprehensive array of characterization techniques was employed, encompassing 2D surface roughness analysis, scanning electron microscopy, X-ray diffraction, nanoindentation, energy-dispersive X-ray spectroscopy and assessments of wear and corrosion performance.

The characterization results of this article reveal a compelling difference between saccharin-free Ni-Cr coatings and their saccharin-modified counterparts. Notably, microcracks, a common occurrence in saccharin-free coatings, were suppressed in the saccharin-modified Ni-Cr coatings. Additionally, the latter exhibited a smoother and more uniform surface texture. A crucial observation was that the introduction of saccharin into the bath was directly associated with an increased incorporation of chromium within the coatings, resulting in higher nanohardness values. Furthermore, the residual stress within the coatings shifted from tensile to compression as saccharin concentrations increased.

Concurrently, surface roughness and wear rates exhibited a consistent downward trend with increasing saccharin concentrations in the solution. The most significant findings were seen in the domain of corrosion resistance. Saccharin-modified Ni-Cr coatings outperformed the bare steel substrate and saccharin-free Ni-Cr coatings. Intriguingly, the enhancement of corrosion resistance was not linearly proportional to saccharin concentration; the optimal corrosion resistance was achieved at a concentration of 1 g/l.

Keywords: *electrodeposition, Ni-Cr alloys, saccharin, hardness, wear, corrosion*

1. Introduction

Nickel-chromium (Ni-Cr) alloys hold a pivotal role in technology and industry. Within this category, Ni-Cr coatings are particularly notable, given the contemporary emphasis on lightweight materials in technology. Chromium (Cr) is commonly alloyed with nickel (Ni) for both decorative and protective purposes. These coatings offer exceptional corrosion resistance and high oxidation resistance, rendering them suitable for diverse environmental conditions [1]. Moreover, the specific properties of Ni-Cr alloys tend to vary on the basis of the ratios of the constituent metals [2].

Electrodeposition emerges as the favoured method for obtaining Ni-Cr alloy coatings, primarily due to its cost-effectiveness, the consistent quality of coatings it produces, and its ability to operate at room temperature [3]. Electrodeposition baths comprise a blend of inorganic and organic salts, acids, or alkalis, along with metal salts [4]. Such baths have the capacity to integrate a variety of organic and inorganic additives. This integration serves to improve the stability of the bath, ensure even distribution of metals, and fine-tune the chemical, physical, or technological attributes of the deposited metal. These attributes encompass qualities like resistance to corrosion hardness, brightness, mechanical robustness, machinability, internal stress management, resistance to wear, and suitability for soldering. It's worth noting that additives, whether organic or inorganic, exhibit their effectiveness within specific concentration

* E-mail: mehmet.demir@iste.edu.tr

ranges [5]. If their concentration exceeds or falls short of these ranges, their impact on the deposition process and the resulting properties of the deposit may vary [4]. Consequently, the use of additives in the bath often involves an experimental dimension [6]. The presence of additives in coating solutions used for the electrodeposition method significantly impacts deposition kinetics, nucleation growth mechanisms, and the formation of residues affecting microstructure [7]. Additives in the electrodeposition process typically serve as catalysts or inhibitors [8]. These functions can be understood in terms of blocking active sites on the substrate, increasing the activation polarization of individual ions, and the propensity of metal ions to form complexes [9]. Additives can be dissolved in water-insoluble or slightly water-soluble organic compounds, facilitating their uniform distribution in the solution. This, in turn, reduces the formation of impurities and prevents the coagulation and sedimentation of suspended solids, which can lead to rough or porous deposits. Additionally, additives inhibit crystal growth, enhancing the final coating's brightness. One such organic additive, saccharin, has a long history of use in electroplating. It serves to mitigate internal stress in deposits, refine particle structures, and improve film quality [10]. In various studies, a range of additives, including saccharin, gelatine, sodium deoxyl sulphate, trimethylamine borane (TMAB), and cetyltrimetylammonium bromide (CTAB), have been examined for their effects. The focus of this study is on the addition of saccharin and its effects on different alloy or composite coatings such as Ni [8, 11], Co [12, 13], CoNi [10, 14], CoPt [15], NiMo [16], ZnNi [17], NiFe [18], NiW [19], NiWP [20] and NiFe/SiC [21]. Tebbakh et al. conducted research on Ni-Co alloy coatings on a ruthenium substrate, in which they added saccharin at various concentrations to the electrolytic bath. They studied the effects on electrochemical deposition, chemical composition, corrosion resistance, and the magnetic and physical characteristics of deposits. Their findings revealed that saccharin altered the deposition process, increased the proportion of Co, and caused grain thinning in the deposit. Furthermore, it improved its corrosion resistance and affected its magnetic properties [10]. Wang et al. [20] investigated electrodeposited NiWP alloy coatings on pure copper substrates with varying saccharin concentrations in the bath (0–6 g/l). The study examined wear resistance, polarization curves, microhardness, and deposition rate. Their results indicated that an increase in saccharin concentration between 2 and 4 g/l enhanced the microhardness, corrosion resistance, and wear resistance of NiWP alloy coatings. However, these properties decreased with the addition of 6 g/l saccharin. Li et al. explored the effects of saccharin on cathodic polarization, cathodic current efficiency, hardness, surface morphology, and internal stress during Ni electrodeposition from a Watt-type coating bath. They observed an increase in cathodic polarization, surface morphology changes, increased stiffness, and reduced tensile stress. However, they noted that these changes were not proportional to the increase in saccharin amount, and the coating properties decreased [22]. Wasekar et al. [8] investigated the impact of current density, deposition mode, and the presence of saccharin as an additive on the microstructure, sulphur content, grain size, and microhardness of nanocrystal line Ni coatings. In their study examining the effect of flow type, they reported a thinning of the coating's grain size when saccharin was present, along with changes in the peak phases, according to subsequent X-ray diffraction (XRD) analysis [8]. Mosavat et al. [17] produced nanocrystal line Zn-Ni alloy coatings in a bath containing saccharin as an additive. They analysed how saccharin concentration and current density affected the coatings' crystallite size and surface roughness, finding that both decreased as saccharin concentration increased [17].

In these studies, it's generally reported that properties like surface roughness decrease, cracks are reduced or eliminated, and smoother, more compact surfaces are achieved with the addition of saccharin. Additionally, saccharin tends to increase coating surface hardness. The increment in corrosion resistance, however, is not strictly proportional to the addition of saccharin. While a moderate increase positively affects corrosion resistance, beyond a certain point, this effect reverses, and further saccharin additions decrease the rate of

improvement. Furthermore, saccharin is known to reduce internal stresses. In various co-deposition studies, the accumulation of secondary elements has been found to increase with higher saccharin amounts.

Despite existing literature supporting the role of saccharin in enhancing properties like surface roughness, hardness values, and corrosion resistance in electrodeposited coatings, no study has explored the impact of saccharin in the electrodeposition of Ni-Cr alloy coatings. This gap in research motivates the current study, which focuses on the role of saccharin in depositing Ni-Cr alloy on a low carbon steel substrate. The study investigates the effect of saccharin (0, 0.5, 1, 2 g/l) addition on the formation characteristics (homogeneity, cracks, surface roughness, etc.), mechanical properties (hardness, residual stress, wear, etc.), and the corrosion resistance of Ni-Cr coatings.

2. Experimental study

The steel substrate, whose chemical composition was analysed using a Thermo Jarrell Ash/Baird DV-6S 3063A spectral analyser (as detailed in Table 1), had dimensions of 15 mm × 15 mm × 5 mm. Ag/AgCl electrodes served as reference electrodes, while platinum wire was employed as the counter electrode in the electroplating bath.

Proper cleaning of the substrate is vital for ensuring robust adhesion between the coating and the substrate, while also preventing adverse effects on the coating deposition process. Contaminants such as rust, dirt, and oil on the substrate's surface can detrimentally impact the composition of the electroplating bath. To prepare the substrate, a multi-step cleaning process was employed. Initially, it was meticulously sanded with emery paper of varying grades (600, 1200, and 2400). Subsequently, the substrate underwent a thorough cleansing with acetone, followed by rinsing with distilled water to eliminate any residual acetone. Further cleaning was achieved through the application of methanol, a mildly alkaline solution, and a final rinse with purified water. The substrate was then subjected to an etching process using a 20% concentrated HCl (hydrochloric acid) solution for 20 seconds, followed by another rinse with distilled water, preparing it for the subsequent deposition process.

Table 1. Chemical composition of steel used in experimental studies

C	Si	Mn	Fe	Pmax	Smax
0.419	0.254	0.751	98	0.040	0.050

Table 2. Electrodeposition conditions

Parameter	Amount
Current density	200 mA/cm^2
Ultrasonic mixing	5 min
Temperature	40°C
Mixing speed	100 rpm
pH	2.5

Table 3. Bath components

Bath solution	Amount	Function
$NiSO_4.7H_2O$ (nickel sulphate)	50 g/l	Ni^{2+} source
$NiCl_2.6H_2O$ (nickel chloride)	45 g/l	Ni^{2+} source
$CrCl_3.6H_2O$ (chromium chloride)	75 g/l	Cr^{3+} source
H_3BO_3 (boric acid)	50 g/l	Blocking agent
$C_6H_8O_7$ (citric acid)	70 g/l	Blocking agent
$Na_3C_6H_5O_7.2H_2O$ (sodium citrate dihydrate)	105 g/l	Complexing agent
$C_7H_4NNaO_3S \bullet 2H_2O$ (sodium saccharin)	0, 0.5, 1, 2 g/l	Additive material

Drawing from pertinent literature, we established suitable electrodeposition conditions and bath components, as documented in Tables 2 and 3 providing valuable insights [23]. Prior to electrodeposition, all bath solutions underwent a uniform mixing process using a Hielscher UP 200 S ultrasonic mixer, set at a 0.5 cycle value and 50% amplitude, for a duration of 5 min.

The electrodeposition of coatings occurred under a consistent current of 200 mA/cm^2, utilizing a Watts-type bath containing 200 mL of electrolyte. The pH of the bath was adjusted to 2.5 through the addition of either H2SO4 or NaOH as needed. The electrolyte temperature was meticulously maintained at 40 ± 1°C throughout the process. The

bath included nickel sulphate and nickel chlorite as sources of nickel, along with chromium chloride as the source of chromium. Boric acid served as a pH regulator, and citric acid functioned as a complexing agent within the bath. The concentration of saccharin in the bath was systematically varied within the range of 0, 0.5, 1, and 2 g/l.

The electrochemical characteristics of the saccharin additive baths were assessed using cyclic voltammetry (CV) with a CHI 608 model device. The scans were conducted within a potential window spanning from 1.5 V to −1.5 V, employing a scan rate of 10 mV/s. For the examination of coating surfaces before and after wear, a Thermo Scientific Apreo S scanning electron microscope (SEM) was employed. This sophisticated instrument features Ultra Dry EDS and Quasor II EBSD detectors, operating at a 30 kV acceleration voltage, and facilitating detailed metallographic analysis. X-ray diffraction (XRD) analyses were executed using a computer-controlled RIGAKU SmartLab device. The 2θ angles of the substrate phases were selected within the range of 5° to 90°, with Cu Kα radiation ($\lambda = 0.154$ nm) used as the X-ray source.

Nanohardness measurements were conducted using a Berkovich probe on a Hysitron TI-950 TriboIndenter device. The Oliver-Pharr analysis method was employed, utilizing a 1×5 analysis matrix [24]. A peak load of 5 mN was applied with a trapezoidal function loaded at a constant rate for 5 sec, held constant for 2 sec, and then gradually increased over 5 sec. To examine the indentations on the coating surfaces, a scanning probe microscope (SPM) was employed. Surface roughness and wear surface depth were determined using a Wave System Hommelwerke T8000 2D profilometer. Measurements were taken over a 4-mm length at a speed of 2 mm/sec.

Dry sliding wear tests were carried out using TurkYus POD & HT & WT device following ball disc type configuration. Tests were performed according to ASTM G99-17 standard [25]. The experiments were carried out with a 6-mm diameter 1917 $HV_{0.05}$ abrasive WC ball under a load of 5 N, a sliding distance of 100 m, a sliding speed of 0.25 m/sec, a rotation speed of 318 rpm, a temperature of 25°C and a relative humidity of 40%. was maintained in the environment. Each sample was tested three times, for wear, for corrosion, and for electrochemical impedance. After the wear test, cross-sectional measurements of the circular wear path were taken at four different points with a 90° angle between them, allowing the determination of wear scar length (L, mm), wear scar volume (V, mm^3), wear scar radius (r, mm), average wear scar depth (D, μm), average wear scar width (W, μm), and wear rate (Wr, mm^3/Nm), as specified in previous studies [26].

For all corrosion tests, a CHI 608E analyser was employed, utilizing a 3.5% NaCl solution identical to the one used during coating acquisition. In this study, three different corrosion measurement methods (OCP, Tafel, AC Impedance) were employed, all conducted at room temperature. The corrosion cell used in the experiments featured a three-electrode configuration comprising a reference electrode, a counter electrode, and a working electrode [27]. Over a span of 3600 seconds, OCP curves were plotted as a function of time. Electrochemical impedance (EIS) tests were conducted within the frequency range of 100 kHz to 10 MHz, employing a 10-mV amplitude. Equivalent circuit analyses were performed using ZsimpWin 3.22 (EChem software, USA), achieving an error rate of less than 10% for all coatings. Potentiodynamic corrosion tests covered the potential range of −250 mV to +250 mV, based on the potential value derived from OCP, with a potential scan rate of 0.1 mV/s. The sample area for all corrosion tests was standardized at 1 cm^2, and tests were repeated in triplicate. Corrosion rate, corrosion current, and corrosion potential values were automatically determined using the software attachment of the CHI 608E device.

3. Results and discussion

3.1. Cyclic voltammetry studies of deposition baths

In Ni-Cr coatings deposited onto AISI 1040 steel substrates, the initiation potentials for coating formation were determined by means of cyclic voltammetry (CV), as illustrated in Figure 1.

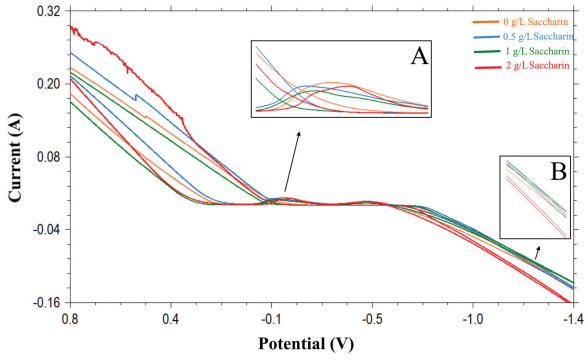

Fig. 1. Alternating voltammetry curves obtained from baths

Notably, the open circuit potential of the solution displayed a positive value in Figure 1, suggesting that the current gradually decreased from 0.28 amps upon the application of a voltage. This decline was not indicative of deposition but rather the formation of hydrogen gas [28]. Upon applying a negative potential of 0.12 V, the current became null and remained constant until reaching −0.6 V. The graph reveals that, after attaining a cathodic potential of −0.6 V, a rapid reduction in cathodic current was observed, signalling the commencement of deposition. In section "B," it's evident that after the drop in current, the curve deviated from the path to −1.4 V and returned from this value. This phenomenon stems from the formation of the Ni-Cr alloy coating during the initial deposition, with continuous modification of the substrate during subsequent cycles. Dissolution occurred on the substrate, and it's noteworthy that accumulation appeared on the platinum wire once the CV cycle was completed.

The dissolution peaks, as depicted in section "A," were noted during the return potentials. The figure underscores that the dissolution peak was most pronounced in the bath without saccharin, with the intensity of the dissolution peak decreasing as saccharin concentration increased. In other words, the migration of the coating to the substrate intensified with higher saccharin content, indicating improved efficiency. In summary, the deposition process was observed to occur within the potential range of 0.12 V to −0.6 V on the test samples.

3.2. Surface and microstructural characterization

Figure 2 presents SEM images of the Ni-Cr coatings, along with EDS results for the entire region shown in the figure. The morphology of the Ni-Cr coatings exhibited a characteristic spherical nodular structure, as commonly observed in dominant Ni coatings [1]. Figure 2a notably reveals the presence of micro-cracks, a typical characteristic of Ni-Cr alloy coatings [29]. These cracks may be attributed to volumetric changes resulting from hydrogen absorption or residual stresses stemming from the formation of multiple phases [30]. It's worth noting that increasing the amount of Cr in the coating can elevate internal stresses and lead to the formation of cracks [31]. The use of additives is an effective strategy to mitigate this undesirable aspect of Ni-Cr coatings [15].

Figures 2b to 2d present SEM images of coatings from baths containing 0.5 g/l saccharin, 1 g/l saccharin, and 2 g/l saccharin, respectively. Notably, the coating in the bath with 0.5 g/l saccharin exhibited a reduction in grain size and the complete closure of cracks (Figure 2b). In the case of the bath with 1 g/l saccharin, the grains displayed a more compact surface, albeit slightly larger than those in the bath with 0.5 g/l saccharin (Figure 2c). This suggests an enhancement in corrosion resistance and surface roughness. However, as the saccharin content increased, pinholes began to appear, indicating a potential adverse effect on corrosion resistance.

Particularly noteworthy is the increase in surface smoothness with higher saccharin content in the electrolyte. This might be attributed to the presence of sulphur in the saccharin molecule, which can release sulphur compounds during electroplating. In the Ni-Cr alloy coating, these dissociated sulphur compounds can lead to volume expansion [32]. Such expansion can induce compressive stresses in the coating, offsetting internal stresses generated during electrodeposition. In particular, the addition of saccharin in the right proportions can reduce internal stresses and minimize crack formation in the coating [20].

Table 4 provides noteworthy insights into the composition of saccharin, particularly the presence

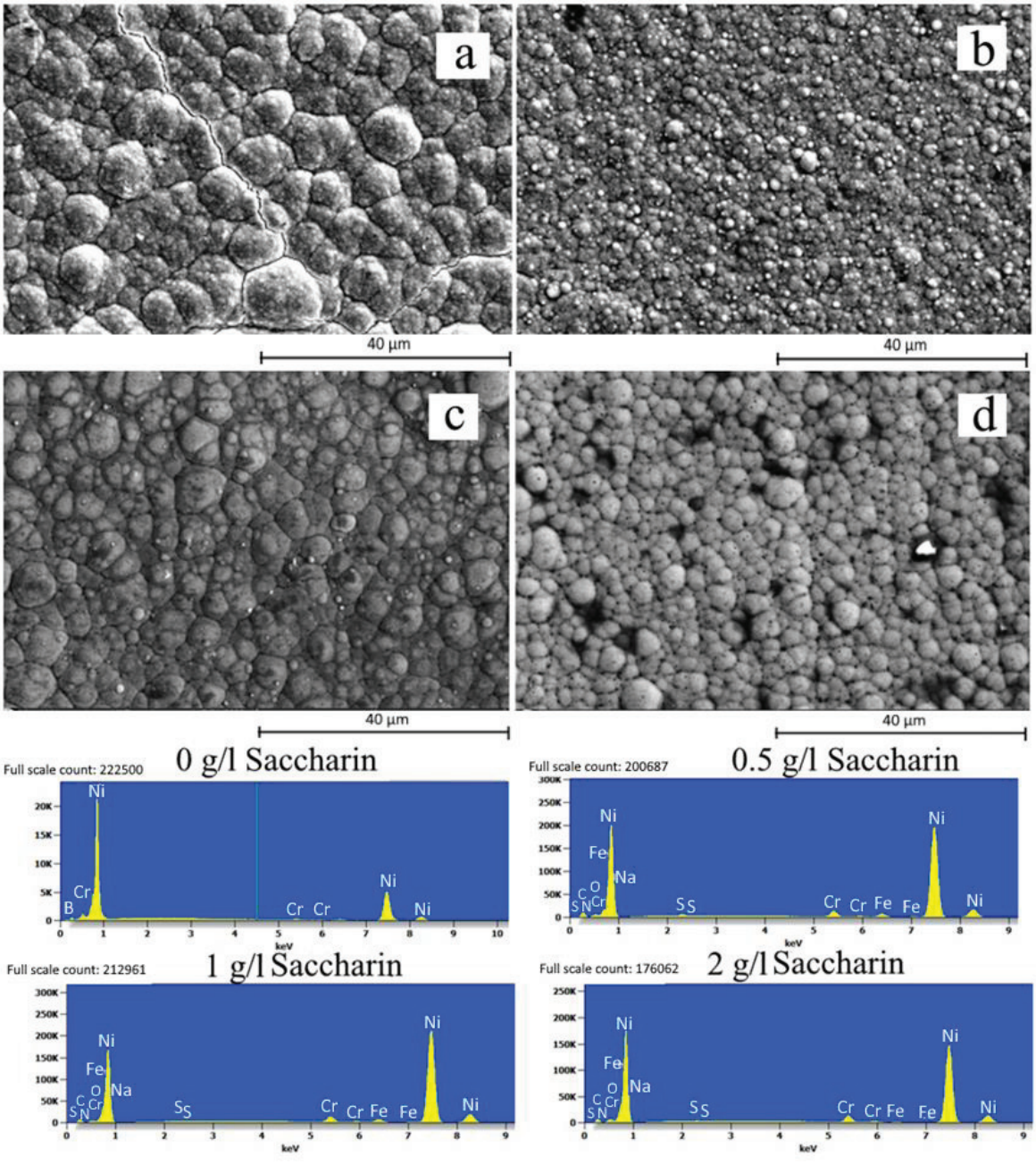

Fig. 2. SEM images and EDS analysis a) 0 g/l saccharin, b) 0.5 g/l saccharin, c) 1 g/l saccharin, d) 2 g/l saccharin

of elements. One of the most striking observations from the table is the substantial increase in the concentration of chromium (Cr) with the addition of saccharin. It becomes evident that the quantity of Cr incorporated into the coating nearly triples with each incremental increase in saccharin concentration. This finding aligns with existing literature, which supports the notion that the inclusion of saccharin in the bath is conducive to enhanced accumulation of auxiliary metals [10].

3.3. Phase analysis (XRD studies)

In this subsection, Figure 3 illustrates the XRD analysis of the coatings, with the corresponding peak angles and DB card numbers presented in

Table 4. Chemical composition of coatings according to EDS analysis (wt. %)

	C	N	O	Na	S	Cr	Ni
0 g/l Saccharin	0.00	0.00	0.00	0.00	0.00	1.18	98.82
0.5 g/l Saccharin	7.83	2.27	1.77	0.17	0.17	2.53	85.27
1 g/l Saccharin	8.64	2.37	0.00	0.13	0.19	2.84	85.83
2 g/l Saccharin	7.87	1.85	0.29	0.19	0.22	3.38	86.21

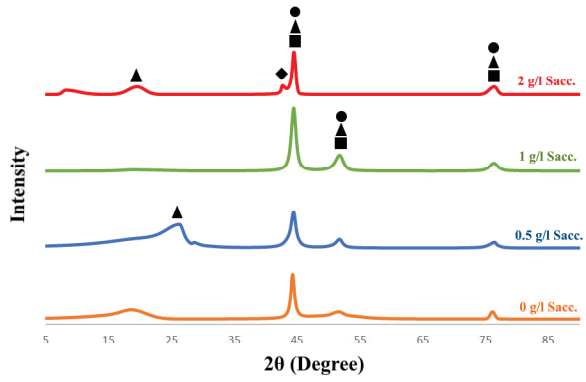

Fig. 3. X-ray diffraction patterns of coatings

Table 5. Notably, the most striking feature is the presence of specific diffraction peaks associated with nickel. At approximately 44.5 (1 1 1), 51.8 (2 0 0), and 76.3 degrees (2 2 0), which correspond to the 2θ values where Ni peaks typically form, an alloy of $(Ni_2Cr_{23})0.16$ was detected. This observation is consistent with findings in the literature [33]. It's worth noting that coatings formed in the presence of 2 g/l saccharin displayed different peak patterns compared to other samples. Specifically, the Cr peak at 51.8 degrees was absent in this coating, while the Cr_7Ni_3 alloy phase emerged at 42.6 degrees. Furthermore, the width of the peak at 76.3 degrees increased with higher saccharin concentrations.

Table 6 provides XRD models, revealing that the grains in the samples are crystalline in nature. The table also facilitates a comparison of the average crystallite grain size. The Scherrer equation was employed to determine the average grain size [34], utilizing the primary peak (111) for all samples. Scherrer equation:

$$D = \frac{\mathrm{k}.\lambda}{\beta \cos\theta} \tag{1}$$

where D is the average particle diameter (in Å), λ is the X-ray radiation wavelength (in Å), K is a constant, θ is the peak angle, and β is the full width at half maximum (FHWM) of the respective XRD peak [34]. Grain size measurements were converted to nanometers (nm). According to the literature, the grain size of the coating obtained from a saccharin-free bath measures 32.42 nm, and it is well-established that the addition of saccharin leads to a reduction in the average crystallite grain size [8, 35]. The smallest grain size was observed in the bath with 0.5 g/l saccharin. As the saccharin content increased, grain sizes progressively increased. Notably, the sample containing 2 g/l saccharin resulted in a grain size identical to that of the sample without saccharin. During electrodeposition, saccharin molecules adhere to active growth sites on the crystal surface, enhancing cathodic polarization in the plating bath. This reinforcement has a positive impact by reducing the rate of nucleation and increasing the formation of nuclei. As a direct consequence, there is a notable reduction in the crystal grain size of the NiCr alloy coating [20]. However, with the continued addition of saccharin to the electrolyte, it caused the grains to grow instead of thinning. This situation is encountered in the literature [36].

3.4. Hardness studies

To assess the impact of saccharin addition on the resulting hardness and elasticity modulus, nanoindentation hardness measurement experiments were conducted. Figure 4 illustrates the nanoindentation loading-displacement curves, while Table 7 presents the data obtained from the nanoindentation tests.

The nanoindentation results revealed that the Ni-Cr alloy coating exhibited a hardness of 1.76 GPa. However, with increasing concentrations of saccharin, the hardness increased to 2.93 GPa. Notably, the load-displacement curve for the sample with 2 g/l saccharin appeared notably narrower compared to the others, indicative of greater hardness. This increase in hardness can be attributed to the smoother surfaces obtained with higher saccharin concentrations in the bath. Furthermore, the growing amount of Cr in the coating was believed

Table 5. Angle values and DB card numbers

	Chemical formula	2-theta (deg)	Phase name	DB card number		Chemical formula	2-theta (deg)	Phase name	DB card number
		18.7	100				44.4	111	
		26.3	110	01-089-2392	■	Ni	51.8	200	00-004-0850
▲	Cr	44.4	210	01-077-7591			76.3	220	
		51.7	200				44.4	111	
		76.3	220		•	$(Cr_2Ni_{23})_{0.16}$	51.8	200	01-077-7616
♦	Cr_7Ni_3	42.6	410	00-051-0637			76.3	220	

Table 6. Parameters obtained from XRD models

Sample	2 (Degree)	Full width at half maximum (FWHM)	Grain size (D) (nm)
0 g/l Saccharin	44.28	0.650	32.42
0.5 g/l Saccharin	44.44	0.960	21.87
1 g/l Saccharin	44.46	0.875	23.99
2 g/l Saccharin	44.47	0.644	32.58

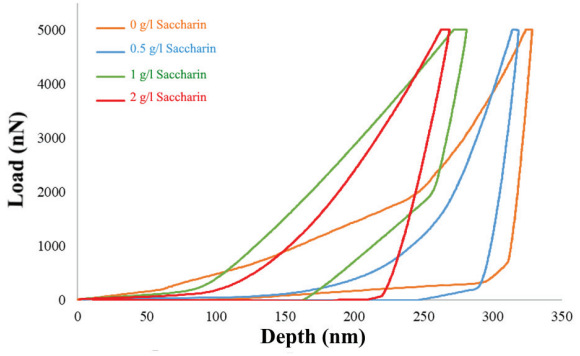

Fig. 4. Nanoindentation load-displacement curves

to have a positive effect on hardness [31]. EDS analysis corroborated this, showing an increase in the accumulation of Cr with higher saccharin content. The observed trend of increasing hardness with the addition of saccharin aligns with findings in the literature [37].

Another significant finding in this study is that adding saccharin, up to 2 g/l, led to a drop in the modulus of elasticity. While saccharin contributed to improved surface properties, it resulted in reduced adhesion of the coating to the substrate. The more compact surface structure correlated with the observed increase in hardness.

Furthermore, this study examined residual stresses to understand why the hardness did not change as expected with variations in grain size. A positive sign signifies tensile stress, while a negative sign indicates compressive stress. Without saccharin in the bath, the sample displayed tensile stress. However, with saccharin added, the residual stress shifted toward compression. It's well-known that hardness decreases with tensile stress [38], offering an explanation for the hardness increase with the addition of saccharin. Equation (2) was used to calculate the residual stresses [39] considering the distribution of hardness (H) and Young's modulus (E), and the maximum indentation depth (h) was determined using the Oliver and Pharr method [40].

$$\frac{P_{max}}{Eh^2} = 5.626\left(\frac{\sigma_y}{E}\right)^{0.5}\left\{1 - \left[3.51\left(\frac{\sigma_y}{E}\right)^{0.5} + 0.032\left(\frac{\sigma_y}{E}\right)^{-0.5}\right]\left(\frac{\sigma_r}{\sigma_y}\right)\right\} \quad (2)$$

If the abbreviations in the table are explained: hc (contact depth), Pmax (max load), s (slope of the unloading curve (dP/dh), A (contact area), hmax (maximum depth), Er (reduced modulus of elasticity). In addition to crystal structure and morphology, surface roughness plays a crucial role in coatings [41]. Figure 5 presents a graph depicting the average surface roughness, highlighting a noticeable reduction in surface roughness with increasing saccharin concentrations. Specifically, the Ra value decreased from 0.32 for the sample without saccharin to 0.1 for the sample with 2 g/l saccharin. This represents a reduction in roughness by more than threefold due to the addition of saccharin. A similar trend was observed for Rz,

Table 7. Elastic modulus, hardness and residual stress values

	h_c (nm)	P_{max} (μN)	S (μN/nm)	A (nm^2)	H_{max} (nm)	E_r (GPa)	H (GPa)	Residual Stress (Gpa)
0 g/l Sacc.	317	5006	326	2842233	329	171.58	1.76	0.51
0.5 g/l Sacc.	304	5005	257	2632610	319	140.58	1.90	0.24
1 g/l Sacc.	250	5007	99	1819289	281	65.17	2.75	−0.95
2 g/l Sacc.	242	5008	136	1706650	269	92.11	2.93	−0.71

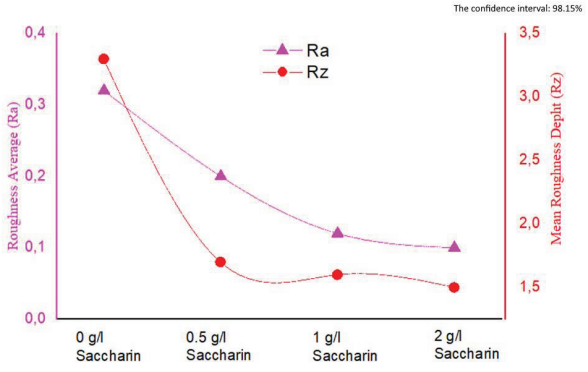

Fig. 5. Effect of saccharin addition on the surface roughness of Ni-Cr coatings

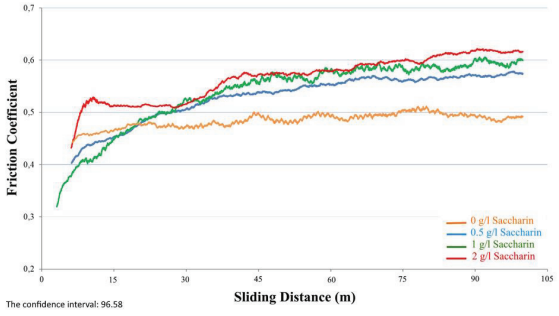

Fig. 6. Friction coefficient of coatings

with a threefold reduction compared to the coating achieved without the inclusion of saccharin in the bath. The primary reason for this phenomenon is the ability of saccharin to flatten the coating surface. With high free adsorption energy, deposition occurs more rapidly on protruding portions of the coating. This results in an increased presence of additives in areas with greater accumulation. This, in turn, reduces electron transfer, leading to enhanced accumulation in regions with lower levels. Consequently, a more uniform coating is achieved. Additionally, coating thicknesses were measured as 10 ± 1 μm.

3.5. Friction coefficient and wear mechanisms

Upon reviewing the friction coefficient graph (Figure 6), it is seen that the addition of saccharin starts with a lower friction coefficient value. Here, the lowest friction coefficient value is in the sample containing 1 g/l saccharin. However, the sample containing 2 g/l saccharin is almost at the same points compared to the sample without saccharin addition. Due to the initial values not being distinctly visible on the graph, their approximately specific values (0 g/l saccharin initial value = 0.45, 2 g/l saccharin initial value = 0.44) are explicitly provided here. As the sliding distance increases, the surface hardness also rises, and correspondingly, the friction coefficient exhibits a continuous increase. Despite having lower roughness, the rise in the friction coefficient over the sliding distance is likely caused by the harder particles detaching from the surface. These particles become trapped between the abrasive ball and the substrate, functioning as abrasives. Conversely, the saccharin-free Ni-Cr sample initiates with a friction coefficient of 0.47 and maintains a stable trajectory.

When examining the SEM image of the microstructure of the worn surface (Figure 7a), it's evident that micro cracks, oriented perpendicular to the wear track, are present. In regions where these micro cracks intensify due to repeated loading, plastic deformation occurs. The size of the plastic deformation measures approximately 40–50 μm in some areas, leading to the effective spilling of the coatings from the surface. Additionally, a complex wear mechanism is observed, characterized by micro scratches and micro smears in the form of

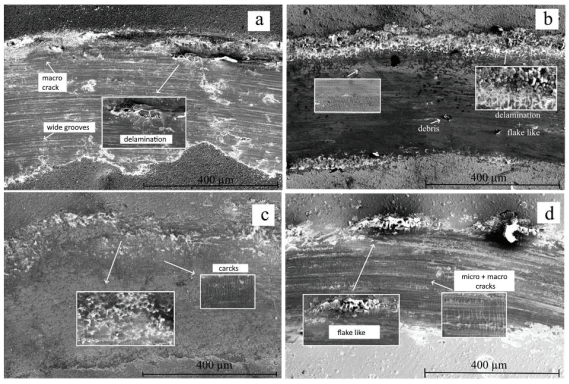

Fig. 7. Worn surface morphology: (a) 0 g/l saccharin, (b) 0.5 g/l saccharin, (c) 1 g/l saccharin, (d) 2 g/l saccharin

wide grooves on the sample surface, parallel to the wear track [42].

In the SEM image of the worn surface of the Ni-Cr coating achieved with 0.5 g/l saccharin (Figure 7b), an oxidation-type wear mechanism is evident in the central and inner regions. Around the edges of the wear marks, surface tearing due to fatigue can be observed, resulting from tensile stresses behind and compression stresses ahead of the abrasive ball. It's also possible that these tears are caused by wear particles, as some areas of the surface exhibit wear debris. In the outermost region, a flaking-type wear mechanism occurs through delamination, a consequence of fatigue resulting from the repeated application of loads [26].

Upon examining the SEM wear images depicted in Figures 7c and 7d, it's noticeable that both exhibit similar wear behaviour. Unlike the other samples, micro cracks oriented perpendicular to the direction of the abrasion scar intensify. Moreover, a darker contrast colour is apparent on the surface, suggesting the formation of an oxidation-type wear mechanism. The increased number of micro cracks is attributed to the higher surface hardness of these samples. Increased hardness reduces toughness and increases fragility. Furthermore, the mismatch between the coating layer and the substrate's hardness or the difference in hardness and modulus of elasticity between the substrate and the Ni-Cr coating layer may account for these observed differences [43].

Table 8. Wear rate, wear volume loss and average COF values

Sample Name	Wear rate (mm^3/Nm) (10^{-6})	Volume loss (mm^3) (10^3)	Coefficient of Friction (COF)
0 g/l saccharin	11.24	5.620	0.483
0.5 g/l saccharin	5.91	2.953	0.528
1 g/l saccharin	4.93	3.002	0.535
2 g/l saccharin	3.75	1.875	0.563

Upon reviewing Table 8, it's evident that the addition of saccharin results in a significant reduction in wear volume losses, with decreases of 1.87 and 3 times observed. This reduction can be attributed to the increased hardness achieved through the addition of saccharin. As the surface hardness of the material increases, the abrasive ball penetrates the surface to a lesser extent, and the removal of abrasive particles during wear is diminished. This, in turn, leads to an enhancement in wear resistance [44, 45]. The coefficient of friction (COF) is the ratio of the friction force to the force pressing on them and is dimensionless.

3.6. Corrosion analyses

The corrosion behaviour of both the substrates and coatings was investigated in a 3.5% NaCl solution. The Tafel extrapolation method was used to determine corrosion currents, corrosion potentials, and corrosion rates, which are presented in Figure 8 and Table 9. Notably, all electrodeposited Ni-Cr coatings displayed superior corrosion resistance compared to the AISI 1040 steel substrate. In comparison to AISI 1040, the Ni-Cr alloy coating exhibited a corrosion potential that was 51 mV more positive. Additionally, the addition of saccharin to the Ni-Cr alloy coating resulted in an improvement in corrosion resistance across all baths. Tafel curves and corrosion rates indicated better performance in all baths with added saccharin compared to the bare AISI 1040 steel substrate. However, the enhancement in corrosion resistance was not directly proportional to the saccharin concentration in the bath. The optimum corrosion resistance was achieved with a 1 g/l saccharin concentration in the bath. This particular

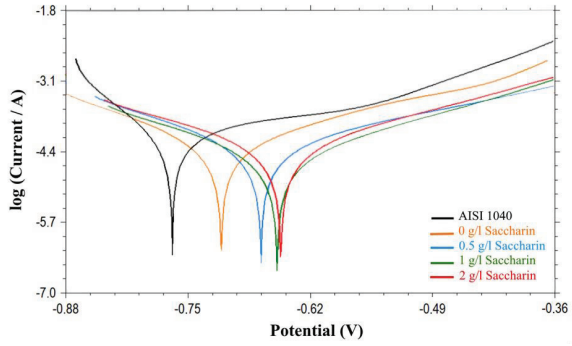

Fig. 8. Tafel curves of coatings and substrate

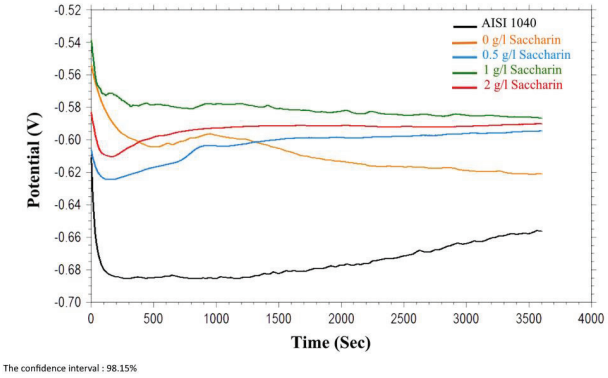

Fig. 9. Open circuit potential curves of Ni-Cr alloy coatings and substrate

Table 9. Corrosion data determined using the Tafel extrapolation method

	ECorr (mV)	**Icorr (μA/cm^2)**	**Corrosion rate (mm/year)**
AISI 1040	−770	91.73	1.08
0 g/l Saccharin	−719	65.18	0.77
0.5 g/l Saccharin	−678	58.26	0.68
1 g/l Saccharin	−662	38.18	0.44
2 g/l Saccharin	−658	56.53	0.66

sample exhibited approximately three times greater corrosion resistance than AISI 1040 steel. Saccharin played a role in diminishing both anodic and cathodic electrochemical reactions responsible for corrosion by altering the coating kinetics. Furthermore, the primary reason for the change in corrosion resistance can be attributed to the elimination of defects on the coating surface facilitated by the addition of saccharin. The additives in the coating served as a physical barrier by filling cracks and micron-sized gaps, partially obstructing reactive areas and reducing cathodic reactions [13]. Additionally, the presence of saccharin within the grain boundaries made the coating less permeable because of its enhanced compactness, offering another explanation for the improvement in corrosion resistance with the addition of saccharin [17]. The existence of imperfections or flaws in the coating may allow the corrosive medium to reach the substrate surface, resulting in an inefficient coating layer that negatively impacts the corrosion protection of the coating [46].

The open-circuit potentials of the steel substrate and Ni-Cr alloy coatings, including those with saccharin, in a 3.5% NaCl solution were recorded for a duration of 3600 seconds (Figure 9). It is known that the one on the positive side of the curves obtained exhibits superior corrosion resistance compared to the others [47]. Figure 9 illustrates that all the coatings displayed improved corrosion resistance compared to the bare AISI 1040 substrate. The more positive Ecorr observed in the coatings may result from various factors, such as the alloy composition of the coating, surface chemistry, reduced surface roughness, and oxidation product within a passive layer produced by the coating. Furthermore, the corrosion resistance of the coatings improved as saccharin was added to the bath, with the coating containing 1 g/l saccharin displaying the best corrosion resistance. Notably, both the coatings and the substrate experienced a rapid decrease in corrosion potential upon exposure to the NaCl solution, which stabilized after a while. The sample without the coating demonstrated the most significant initial drop in potential when exposed to a corrosive environment. Although the Ni-Cr coating initially exhibited a favourable potential, over time, this potential significantly declined. In contrast, the saccharin-added baths initially caused a decrease in potential, but they quickly formed an anti-corrosion layer, effectively protecting the material against corrosion. Consequently, it can be concluded that saccharin, forming an inert physical barrier, is a primary reason for the increased resistance to corrosion. The presence of sulphur accumulating

Table 10. Equivalent circuit parameters

	R_s ($\Omega.cm^2$)	R_p ($\Omega.cm^2$)	n	$Y_o(10^{-4})$ ($\Omega^{-1}.cm^{-2}.sn$)	C_P ($\mu F/cm^2$)
AISI 1040	214	2328	0.42	5.85	89.6
0 g/l Saccharin	161	2615	0.53	6.08	91.8
0.5 g/l Saccharin	195	4371	0.67	2.95	33.4
1 g/l Saccharin	145	5520	0.67	2.70	32.9
2 g/l Saccharin	166	5472	0.59	2.67	34.7

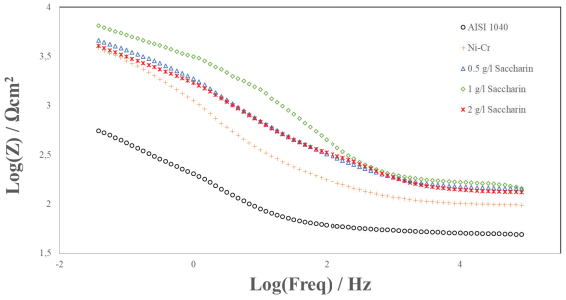

Fig. 10. (a) Nyquist diagrams, (b) impedance modulus plots, (c) bode diagrams, (d) equivalent circuit diagram

at the grain boundaries was found to provide positive results against corrosion when maintained at a certain level. However, an excess of sulphur led to negative corrosion results. Additionally, the coatings' active area decreased as a result of the addition of saccharin [13].

The impedance modulus graph, shown in Figure 10, is a known indicator of corrosion resistance, where an increasing impedance modulus signifies better corrosion resistance [48]. In line with this, it's evident that the sample with the highest impedance modulus is the one with 1 g/l saccharin added to the bath, while the lowest impedance was recorded for the AISI 1040 substrate. This observation supports the presence of a protective barrier between the substrate and the coatings. In all the samples, impedance exhibited a sharp decrease with increasing frequency. However, as the frequency increased further, the impedance began to stabilize. In this region, samples with added saccharin were very close to each other.

Solution resistances (Rs), charge transfer resistances (Rp) of electrode reactions, and double-layer non-ideal capacitances (Cp) were calculated from the EIS data and are provided in Table 10. It's worth noting that the surface shape plays a significant role in altering Cp values. A high density of microcracks and an uneven structure result in a larger contact area. Based on the data, the sample containing 1 g/l saccharin exhibited the most favourable Cp value. However, the addition of more than 1 g/l saccharin resulted in a slight increase in the Cp value. Nevertheless, this increase is relatively modest and is approximately three times lower than the coatings without saccharin addition. This decrease in Cp can be attributed to the improvement in surface properties achieved with the addition of saccharin.

In summary, the steel substrate exhibited inferior corrosion resistance compared to the Ni-Cr alloy coatings in all three corrosion measurement methods. The corrosion resistance of the resulting coatings was enhanced by the addition of saccharin to the electrolytic Ni-Cr alloy bath. However, there was a slight reduction in corrosion resistance when saccharin was added to the bath at concentrations exceeding the optimal level (>1 g/l). In essence, these coatings effectively shielded the substrate from the corrosive environment, thus safeguarding it against corrosion. Saccharin played a key role in forming a physical barrier by filling cracks and gaps on the coating's surface. Additionally, it minimized imperfections, resulting in a denser and less permeable Ni-Cr coating. The uniform structure achieved with saccharin not only improved the coating's corrosion resistance by inhibiting matrix dissolution but also increased its strength. It's worth noting that the decline in corrosion resistance with 2 g/l saccharin can be attributed to the presence of pinhole gaps in the coating. This observation aligns with the SEM images depicted in Figure 2, illustrating a more compact surface and the presence of pinhole cavities due to the addition of 2 g/l saccharin.

4. Conclusions

In this study, we investigated the effects of adding saccharin to the bath in concentrations of 0.5, 1, and 2 g/l on the Ni-Cr alloy coatings obtained through electrodeposition. The following key findings were obtained:

1. Successful deposition of saccharin on AISI 1040 steel was achieved, and the influence of the amount of saccharin on the coatings depended on the electrolyte concentration.
2. Electrochemical behaviour, as determined by cyclic voltammetry (CV), displayed a stable single peak on the positive side for all samples, indicating the bath's stability.
3. Characteristic cracks observed in Ni-Cr alloy coatings, common to this type of coating, were effectively eliminated when saccharin was added to the Ni-Cr bath. This resulted in improved coating surface quality and uniformity.
4. X-ray diffraction (XRD) results revealed distinct peak distributions with varying saccharin concentrations. While nickel-specific diffraction peaks were consistent in all XRD experiments, different peaks emerged in the coating produced with 2 g/l saccharin, setting it apart from the other samples.
5. The hardness values of Ni-Cr coatings increased, and there was a transition from tensile to compressive residual stresses with the addition of saccharin.
6. Saccharin's ability to fill grain boundaries and eliminate crack-related issues led to coatings with enhanced morphology, hardness properties, and improved wear resistance.
7. Wear mechanisms were diverse, with delamination-type wear observed in Ni-Cr alloy coatings, fatigue-type wear in samples containing 0.5 g/l saccharin, and oxidation-type wear in samples containing 1 and 2 g/l saccharin.
8. The sample with 1 g/l saccharin exhibited the best corrosion resistance, although all Ni-Cr deposited samples demonstrated superior corrosion resistance compared to raw AISI 1040 steel.

Acknowledgements

Mehmet Demir would like to express gratitude to The Scientific and Technological Research Council of Turkey (TUBITAK-BIDEB) for their invaluable support through a scholarship granted under the 2211-C program, which greatly facilitated the completion of their Ph.D. studies.

References

[1] Firouzi-Nerbin H Nasirpouri F, Moslehifard E. Pulse electrodeposition and corrosion properties of nanocrystalline nickel-chromium alloy coatings on copper substrate. *J Alloys Compd*. 2020;822:153712. doi: 10.1016/j.jallcom.2020.153712

[2] Sheibani Aghdam A, Allahkaram SRR, S. Mahdavi SRR. Corrosion and tribological behavior of Ni-Cr alloy coatings electrodeposited on low carbon steel in Cr (III)-Ni (II) bath. *Surf Coat Technol*. 2015;281:144–9. 2015, doi: 10.1016/j.surfcoat.2015.10.006

[3] Akhtar K, Khan KU, Gul M, Zubair N, Shah SSA. Electrodeposition and characterization of Ni-Al2O3 nanocomposite coatings on steel. *J Mater Eng Perform*. 2018;27(6):2827–37. doi: 10.1007/s11665-018-3346-2

[4] Kanani N. Electrolytes for the deposition of metal coatings. *Electroplating*. 2004;55–85. doi: 10.1016/b978-185617451-0/50003-8

[5] Schlesınger M, Paunovıc M, eds. *Modern electroplating*, 5th ed. New Jersey: John Wiley & Sons, Inc., 2010.

[6] Djokic PL, Stojan S, Cavalloti, Electrodeposition' in *Modern apects of electrochemistry*, no. 12. Singapore: Springer, p. 251–91. doi: 10.1007/978-1-4419-5589-0

[7] Altamirano-Garcia L, Vazquez-Arenas J, Pritzker M, Luna-Sánchez R, Cabrera-Sierra R. Effects of saccharin and anions (SO42-, Cl-) on the electrodeposition of Co–Ni alloys. *J Solid State Electrochem.* 2014;19(2): 423–33, 2014, doi: 10.1007/s10008-014-2616-7

[8] Wasekar NP, Haridoss P, Seshadri SK, Sundararajan G. Influence of mode of electrodeposition, current density and saccharin on the microstructure and hardness of electrodeposited nanocrystalline nickel coatings. *Surf Coat Technol*. 2016;291:130–40. doi: 10.1016/j.surfcoat.2016.02.024

[9] Das MK, et al. Effect of saccharin sodium on the microstructure and hardness of electrodeposited Ni-W coatings. *Key Eng Mater*. 2015;659:535–9. doi: 10.4028/www.scientific.net/KEM.659.535

[10] Tebbakh S, Messaoudi Y, Azizi A, Fenineche N, Schmerber G, Dinia A. The influence of saccharin on the electrodeposition and properties of Co-Ni alloy thin films. *Trans Inst Met Finish.* 2015;93(4):196–204. doi: 10.1179/0020296715Z.000000000247

[11] Mockute D, Bernotiene G, Vilkaite R. Reaction mechanism of some benzene sulfonamide and saccharin

derivatives during nickel electrodeposition in Watts-type electrolyte. *Surf Coat Technol*. 2002;160(2–3):152–7. doi: 10.1016/S0257-8972(02)00385-7

[12] Pan B, Yang Y, Zhang Y, Zhang Q. Effects of saccharin and tetramethylammonium bromide on the microstructure and microhardness of thick cobalt electrodeposits. *Surf Coat Technol*. 2017;329:49–54. doi: 10.1016/j.surfcoat.2017.09.026

[13] Sekar R. Effect of saccharin and thiourea on electrodeposition of cobalt and characteristics of deposits. *Trans Inst Met Finish.* 2015;93(1):44–52. doi: 10.1179/0020296714Z.000000000194

[14] Singh DK, Tripathi MK, Singh VB. Electrolytic preparation of Ni-B 4 C composite coating and its characterization. *J Mat Eng Perform.* 2015. doi: 10.1007/s11665-015-1396-2

[15] Tabakovic I, Qiu J-M, Dragos O. Electrodeposition of thin CoPt films with very high perpendicular anisotropy from hexachloroplatinate solution: effect of saccharin additive and electrode substrate. *J Electrochem Soc*. 2016;163(7):D287–D294. doi: 10.1149/2.0491607jes

[16] Hu J, Zheng XG, Shi Y-N, Lu K. Effect of a mixture of saccharin and 2-butyne-1,4-diol on electrodeposition of nano-grained Ni-Mo alloys. *J Electrochem Soc*. 2017;164(6):D348–53. doi: 10.1149/2.1641706jes

[17] Mosavat SH, Bahrololoom ME, Shariat MH. Electrodeposition of nanocrystalline Zn-Ni alloy from alkaline glycinate bath containing saccharin as additive. *Appl Surf Sci*. 2011;257(20):8311–6. doi: 10.1016/j.apsusc.2011.03.017

[18] Nakamura K, Hayashi T. Effects of saccharin on the elelctrodeposition of Ni-Fe alloy films. *Bull Univ Osaka Prefect,. Sers A Eng Natur Sci.* 1983;32(1):27–36.

[19] Zheng M, Hilty RD. The synergic impact of saccharin and 2-butyne 1,4 diol on the electrodeposition of nanocrystalline NiW alloy. 2010;25(41):117–23. doi: 10.1149/1.3422505

[20] Wang Y et al. Effect of saccharin on the structure and properties of electrodeposition NiWP alloy coatings. *J Mater Eng Perform*. 2016;25(10):4402–7. doi: 10.1007/s11665-016-2298-7

[21] Ataee-Esfahani H, Vaezi MR, Nikzad L, Yazdani B, Sadrnezhaad SK. Influence of SiC nanoparticles and saccharin on the structure and properties of electrodeposited Ni-Fe/SiC nanocomposite coatings. *J Alloys Compd*. 2009;484(1–2):540–4. doi: 10.1016/j.jallcom.2009.04.146

[22] Li YW, Huang XX, Yao JH, Deng XS. Effect of saccharin addition on the electrodeposition of nickel from a Watts-type electrolyte. *Adv Mat Res*. 2011;189–93:911–4. doi: 10.4028/www.scientific.net/AMR.189-193.911

[23] Demir M, Kanca E, Karahan IH. Characterization of electrodeposited Ni – Cr/hBN composite coatings. *J Alloys Compd*. 2020;844:155511. doi: 10.1016/j.jallcom.2020.155511

[24] Yang F, Li JCM. *Micro and Nano Mechanical Testing of Materials and Devices*. New York: Springer, 2008.

[25] World Trade Organization Technical Barriers to Trade (TBT) Committee. Standard Test Method for Wear Testing with a Pin-on-Disk Apparatus. 2023. doi: 10.1520/G0099-17

[26] Günen A, Kurt B, Milner P, Gök MS. Properties and tribological performance of ceramic-base chromium and vanadium carbide composite coatings. *Int J Refract Metals Hard Mater*. 2019;81:333–44. doi: 10.1016/j.ijrmhm.2019.03.019

[27] Coþkun MI, Karahan IH, Golden TD, Computer assisted corrosion analysis of hydroxyapatite coated CoCrMo biomedical alloys. *Surf Coat Technol*. 2015;275:e1–e9. doi: 10.1016/j.surfcoat.2015.05.037

[28] Meudre C, Ricq L, Hihn JY, Moutarlier V, Monnin A, Heintz O. Adsorption of gelatin during electrodeposition of copper and tin-copper alloys from acid sulfate electrolyte. *Surf Coat Technol*. 2014;252:93–101. doi: 10.1016/j.surfcoat.2014.04.050

[29] Tavoosi M, Barahimi A. Corrosion behavior of amorphous – nanocrystalline Fe – Ni – Cr electrodeposited coatings. 2017;8:103–11.

[30] Wu W, Eliaz N, Gileadi E. Electrodeposition of Re-Ni alloys from aqueous solutions with organic additives. *Thin Solid Films*. 2016;616:828–37. doi: 10.1016/j.tsf.2016.10.012

[31] Huang CA, Lin CK, Chen CY. Hardness variation and corrosion behavior of as-plated and annealed Cr-Ni alloy deposits electroplated in a trivalent chromium-based bath. *Surf Coat Technol*. 2009;203(24):3686–91. doi: 10.1016/j.surfcoat.2009.05.047

[32] Sadeghi; A. Microstructure evolution and strengthening mechanism in Ni-based composite coatings. PhD thesis. Chemnitz Univesity of Technology Germany; 2016.

[33] Suswanto BAK, Suchaimi M, Purwaningsih H, Rochiem R. Pengaruh jarak nozzle pada proses coatıng fecrbmnsi dengan metode wire arc spray terhadap ketahanan thermal. *Prosiding Seminar Nasional Sains dan Teknologi, Tahun*. 2017;35–40.

[34] Pillai AM, Rajendra A, Sharma AK. Electrodeposited nickel-phosphorous (Ni-P) alloy coating: an in-depth study of its preparation, properties, and structural transitions. *J Coat Technol Res*. 2012;9(6):785–97. doi: 10.1007/s11998-012-9411-0

[35] Hassani S, Raeissi K, Golozar MA. Effects of saccharin on the electrodeposition of Ni-Co nanocrystalline coatings. *J Appl Electrochem*. 2008;38(5):689–94. doi: 10.1007/s10800-008-9488-4

[36] Kim SH, et al., Effect of saccharin addition on the microstructure of electrodeposited Fe-36 wt.% Ni alloy. *Surf Coat Technol*. 2005;199(1):43–8. doi: 10.1016/j.surfcoat.2004.11.035

[37] Rezaei-Sameti M, Nadali S, Falahatpisheh A, Rakhshi M. The effects of sodium dodecyl sulfate and sodium saccharin on morphology, hardness and wear behavior of Cr-WC nano composite coatings. *Solid State Commun*. 2013;159:18–21. doi: 10.1016/j.ssc.2013.01.019

[38] Huber N, Heerens J. On the effect of a general residual stress state on indentation and hardness testing. *Acta Mater*. 2008;56(20):6205–13. doi: 10.1016/j.actamat.2008.08.029

[39] Delgado-Brito AM, Contla-Pacheco AD, Castrejón-Sánchez VH, López-Suero H, Oseguera-Peña J, Campos-Silva I. Effect of the diffusion annealing process on the sliding wear resistance of cobalt boride layer. *J Mater Eng Perform*. 2020;29(1):109–25. doi: 10.1007/s11665-019-04538-6

[40] Oliver WC, Pharr GM. An improved technique for determining hardness and elastic modulus using load and displacement sensing indentation experiments. *J Mater Res.* 1992;7:1564–83. doi: 10.1177/003591571901200704

[41] Shahri Z, Allahkaram SR, Zarebidaki A. Electrodeposition and characterization of Co-BN (h) nanocomposite coatings. *Appl Surf Sci*. 2013;276:174–81. doi: 10.1016/j.apsusc.2013.03.062

[42] Günen A, et al. High temperature wear behavior of the surface-modified externally cooled rolls. *Surf Coat Technol*. 2018;348:130–41. doi: 10.1016/j.surfcoat.2018.04.071

[43] Günen A, et al., Effect of borotitanizing on microstructure and wear behavior of Inconel 625. *Surf Coat Technol*. 2017;311:374–82. doi: 10.1016/j.surfcoat.2016.12.097

[44] Wasekar NP, Bathini L, Ramakrishna L, Rao DS, Padmanabham G. Pulsed electrodeposition, mechanical properties and wear mechanism in Ni-W/SiC nanocomposite coatings used for automotive applications. *Appl Surf Sci*. 2020;527:146896. doi: 10.1016/j.apsusc.2020.146896

[45] Liu C, Huang X, Xu R, Mai Y, Zhang L, Jie X. Microstructure and properties of nanocrystalline Ni-Mo coatings prepared by ultrasound-assisted pulse electrodeposition. *J Mater Eng Perform*. 2021;30(4):2514–25. doi: 10.1007/s11665-021-05570-1

[46] Oliveira JAM, de Almeida AF, Campos ARN, Prasad S, Alves JJN, de Santana RAC. Effect of current density, temperature and bath pH on properties of Ni–W–Co alloys obtained by electrodeposition. *J Alloys Compd*. 2021;853:147104. doi: 10.1016/j.jallcom.2020.157104

[47] Tozar A, Karahan IH. A comprehensive study on electrophoretic deposition of a novel type of collagen and hexagonal boron nitride reinforced hydroxyapatite/chitosan biocomposite coating. *Appl Surf Sci*. 2018;452:322–36. doi: 10.1016/j.apsusc.2018.04.241

[48] Buckley DH. *Surface effects in adhesion, friction, wear and lubrication*, vol. 85, no. 2. Ohio: Elsevier, 1981. doi: 10.1016/0043-1648(83)90069-8

Received 2023-11-08
Accepted 2023-12-26